Nozaki-Bekki solitons in semiconductor lasers

https://doi.org/10.1038/s41586-023-06915-7

Received: 27 April 2023

Accepted: 29 November 2023

Published online: 24 January 2024



Check for updates

Nikola Opačak^{1,2, D}, Dmitry Kazakov², Lorenzo L. Columbo³, Maximilian Beiser¹, Theodore P. Letsou^{2,4}, Florian Pilat¹, Massimo Brambilla⁵, Franco Prati⁶, Marco Piccardo^{2,7,8}, Federico Capasso² & Benedikt Schwarz^{1,2 ⊠}

Optical frequency-comb sources, which emit perfectly periodic and coherent waveforms of light¹, have recently rapidly progressed towards chip-scale integrated solutions. Among them, two classes are particularly significant—semiconductor Fabry-Perót lasers²⁻⁶ and passive ring Kerr microresonators⁷⁻⁹. Here we merge the two technologies in a ring semiconductor laser^{10,11} and demonstrate a paradigm for the formation of free-running solitons, called Nozaki-Bekki solitons. These dissipative waveforms emerge in a family of travelling localized dark pulses, known within the complex Ginzburg-Landau equation¹²⁻¹⁴. We show that Nozaki-Bekki solitons are structurally stable in a ring laser and form spontaneously with tuning of the laser bias, eliminating the need for an external optical pump. By combining conclusive experimental findings and a complementary elaborate theoretical model, we reveal the salient characteristics of these solitons and provide guidelines for their generation. Beyond the fundamental soliton circulating inside the ring laser, we demonstrate multisoliton states as well, verifying their localized nature and offering an insight into formation of soliton crystals¹⁵. Our results consolidate a monolithic electrically driven platform for direct soliton generation and open the door for a research field at the junction of laser multimode dynamics and Kerr parametric processes.

Dissipative temporal solitons—stable solitary localized pulses emerge universally in extended nonlinear media, sustained by a dual balance between the nonlinearity and dispersion and diffusion, as well as between the gain and dissipation of the system¹⁶. Their prime examples in optics come from passively mode-locked lasers¹⁷, optical fibres 18,19 and passive microresonators with a high quality (Q) factor 7,20 . Microresonators are of special interest for integrated photonics owing to their compact size and have therefore gained considerable attention. Fine-tuning of the requisite continuous-wave (CW) optical pump, combined with a bulk Kerr nonlinearity, is necessary to provide the parametric gain that leads to bright or dark microresonator solitons 8,9,21. When outcoupled, the circulating soliton results in a periodic train of short pulses, generating a broad frequency comb in the spectral domain¹. These miniature Kerr combs have been the vanguard of microresonator technology, finding use in telecommunication²², ranging²³, high-precision spectroscopy²⁴ and frequency synthesis²⁵.

In this work, we demonstrate a type of optical dissipative solitonsnamed Nozaki-Bekki (NB) solitons-in an electrically driven midinfrared (MIR) ring semiconductor laser. They arise as localized waveforms in a family of travelling dark pulses that satisfy ring periodic boundary conditions. The active laser gain material in our devices simultaneously provides a giant Kerr nonlinearity and eliminates the external optical pump and its challenging frequency tuning, which is a vital ingredient for microresonator combs. The NB soliton regime emerges spontaneously and is directly accessed solely by tuning the laser driving current, which we validate by using a phase-sensitive measurement. The experimental findings are corroborated by a complementary theoretical Maxwell-Bloch formalism with numerical simulations. allowing us to identify favourable dispersive and nonlinear conditions for NB soliton formation and their coherent control. Our initial prediction of their existence originated from the well-known cubic complex Ginzburg-Landau equation (CGLE), which describes spatially extended systems close to bifurcations¹². Although their stability has long been discussed within the CGLE framework, NB solitons have so far been scarcely observed in experiments. Unequivocal classification of NB solitons is made possible by their striking salient characteristicsanti-phase synchronization of the soliton with the primary mode and a 2π temporal phase ramp across the soliton. The localized nature of NB solitons is conclusively demonstrated by further observing multisoliton states, both in theory and experiments. Our findings herald a generation of monolithically integrated self-starting soliton generators that lie at the intersection of semiconductor lasers and Kerr microresonators.

To study NB solitons, we use quantum cascade lasers (QCLs)compact and efficient devices that emit in the MIR and terahertz regions^{26,27}-embedded in a ring cavity. Ultrafast intersubband transitions of QCLs provide not only the optical gain but also a giant Kerr

¹Institute of Solid State Electronics, TU Wien, Vienna, Austria. ²Harvard John A. Paulson School of Engineering and Applied Sciences, Harvard University, Cambridge, MA, USA. ³Dipartimento di Elettronica e Telecomunicazioni, Politecnico di Torino, Turin, Italy. Department of Electrical Engineering and Computer Science, Massachusetts Institute of Technology, Cambridge, MA, USA. ⁵Dipartimento di Fisica Interateneo and CNR-IFN. Università e Politecnico di Bari, Bari, Italy. ⁶Dipartimento di Scienza e Alta Tecnologia, Università dell'Insubria, Como, Italy, ⁷Department of Physics, Instituto Superior Técnico, Universidade de Lisboa, Lisbon, Portugal. 8 Instituto de Engenharia de Sistemas e Computadores - Microsistemas e Nanotecnologias (INESC MN), Lisbon, Portugal, [™]e-mail: nikola.opacak@tuwien.ac.at; benedikt.schwarz@tuwien.ac.at

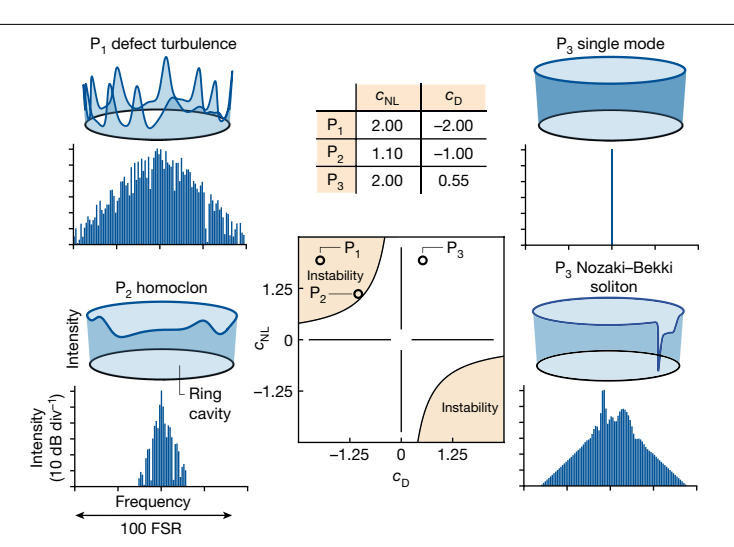
nonlinearity^{28,29}, which is several orders of magnitude larger than in bulk III-V compounds³⁰. This is already exploited for frequency-comb formation in Fabry–Pérot QCLs^{2,6,28}. There, the multimode operation originates from the spatial hole burning (SHB)6, which describes inhomogeneous gain saturation due to a standing wave inside the cavity. caused by the counterpropagating components of the electric field. Conversely, a ring cavity has no reflection points and supports unidirectional field propagation—preventing SHB. Nevertheless, recent work has demonstrated multimode unidirectional ring QCLs due to phase turbulence at low pumping levels, making SHB non-essential¹⁰. Since then, substantial efforts have been made towards developing Kerr combs in ring QCLs^{11,31,32}, leading to bright pulses after spectral filtering³³ and theoretically predicted optically driven solitons^{34,35}—already anticipating the potential of these devices as an on-chip soliton platform. We can interpret ring QCL multimode dynamics on the grounds of the CGLE with periodic boundary conditions¹⁰. Starting from the more general laser master equation⁶, we derive the cubic CGLE

$$\partial_t E = E + (1 + ic_D)\partial_z^2 E - (1 + ic_{NL})|E|^2 E,$$
 (1)

where E is the unidirectional electric field, t is time and z is the spatial coordinate along the ring cavity (see the derivation in Supplementary Information). The entire parameter space is elegantly constricted to just two dimensions, which refer to the dispersive (c_D) and nonlinear (c_{NI}) effects. In lasers, c_D is partly determined by the cavity group velocity dispersion (GVD) k''. Another contribution to the total GVD originates from the gain lineshape, defined with the linewidth enhancement factor (LEF)—a crucial semiconductor laser parameter that describes light amplitude-phase coupling 36,37 . Moreover, the LEF also defines $c_{
m NL}$ and phenomenologically describes the giant resonant Kerr nonlinearity of QCLs^{6,28}. A linear stability analysis of the CGLE divides the c_D - c_{NI} space into two regions depending on the stability of the single-mode CW solution under small perturbations¹² (Fig. 1). Deep within the unstable region, defect turbulence occurs, characterized by a broad, unlocked spectrum and chaotically evolving intracavity intensity (point P₁). Closer to the stable region, the laser undergoes phase turbulence represented by a narrower spectrum and shallow intensity variations (point P_2). Phase turbulence can eventually lead to frequency combs in the form of localized coherent pulse-like structures named homoclons 10,12.

The stable region of the parameter space sustains single-mode operation. However, we show that multimode emission can exist even here if we allow for large perturbations that are beyond the scope of linear stability analysis. The resulting frequency combs—known as NB holes in the CGLE framework¹²⁻¹⁴—have a smooth and broad spectral envelope. In the temporal domain, they correspond to a family of travelling, localized dark pulses that preserve their shape and connect two stable CW fields, giving a constant background. These waveforms exist in a narrow region of the parameter space, and have been so far related to dark solitons³⁸ and experimentally observed in chemical systems³⁹, fluids⁴⁰ and long-cavity ring lasers 41,42. In numerical simulations imposing ring periodic boundary conditions, states comprising an arranged hole and shock pair are structurally stable even with inclusion of higher-order nonlinear terms that are not accounted for in the cubic CGLE and that have a role in real physical systems, for example, lasers 13,43,44. The coexistence of a stable CW field and a hole-shock pair (point P₃) is a prime example of the phenomenon of multistability-stochastic dependence of the laser state on the starting conditions-thus corroborating the solitonic nature of these dissipative localized structures^{7,16}, referred to hereafter as NB solitons in our lasers.

A microscope image of the ring QCL is seen in Fig. 2a, along with an integrated waveguide coupler. The waveguide core is made from the same QCL material and has separate contacts for independent electrical driving. This allows to tune the mode indices, the Q factor, the power of the extracted light, and the coupling between the waveguide and the ring, making this configuration an ideal testbed for a plethora



The unidirectional intracavity intensities and the spectra are obtained from numerical simulations of the CGLE for different points indicated in the parameter space, where the frequency axis of the spectra is normalized to the free spectral range (FSR) of the cavity. The left column shows two states triggered by turbulence inside the CW linearly unstable yellow region of the parameter space (defined by $1 + c_D c_{NL} < 0$), where a single-mode field cannot exist as a steady state. Defect turbulence occurs deep inside the unstable region (point P_1) and is aperiodic, showing chaotic temporal evolution. Close to the border of CW stability (point P_2), phase turbulence leads to narrowband homoclon frequency combs¹⁰. The right column shows the coexistence (multistability) of a single-mode regime and an NB soliton, both set in the CW

linearly stable part of the parameter space $(1 + c_D c_{NL} > 0)$. NB solitons emerge as

coherent, unidirectional propagating dark pulses, characterized by a broad

stabilizing the waveform in ring periodic boundary conditions.

and smooth spectral envelope. The visible pulse shoulder represents a shock,

Fig. 1 | Parameter space of the CGLE with corresponding laser regimes.

of resonant electromagnetic phenomena⁴⁵. The light outcoupling in previous experiments relied on the minuscule ring-bending losses, thus limiting the extracted power to submilliwatt levels at room temperature¹⁰. Using the waveguide coupler to efficiently extract the light, our devices reach power levels above 10 mW (Fig. 2b), bringing them on par with Fabry–Pérot QCLs of a similar ridge length and width, fabricated from the same wafer⁴⁵. While the coupling waveguide is biased below the lasing threshold, the ring QCL is driven above it, where it operates in a unidirectional regime after the symmetry-breaking point^{33,45}. We find that at currents partially higher than the lasing threshold $J_{\rm th}$ (around $1.2J_{\rm th}$), the ring laser emits a multimode field with a narrow beatnote (Fig. 2c). This implies a high degree of coherence, typical of a frequency comb.

To benchmark comb operation, we employ Shifted Wave Interference Fourier Transform Spectroscopy (SWIFTS) – an experimental technique that extracts both the amplitude and the phase of spectral modes⁴⁶. The measured intensity spectrum (Fig. 2d) consists of a strong primary mode surrounded by weaker side modes that form a smooth envelope, strikingly reminiscent of soliton spectra in microresonators^{7-9,20,21}. The intermode phases—the phase differences between adjacent modes-are shown below the intensity spectrum. They are all synchronized in-phase, except around the primary mode, where $\boldsymbol{\pi}$ jumps indicate destructive interference due to anti-phase synchronization. This is evident from the reconstructed intensity profile (Fig. 2e), where a single dark pulse circulates around the cavity in an otherwise quasi-constant CW background-consistent with the predicted fundamental NB soliton. Residual intensity oscillations are due to the limited detection bandwidth. Within the width of the NB soliton, the temporal phase shows a steep ramp covering 2π and remains linear everywhere else, proving that the CW background around the soliton

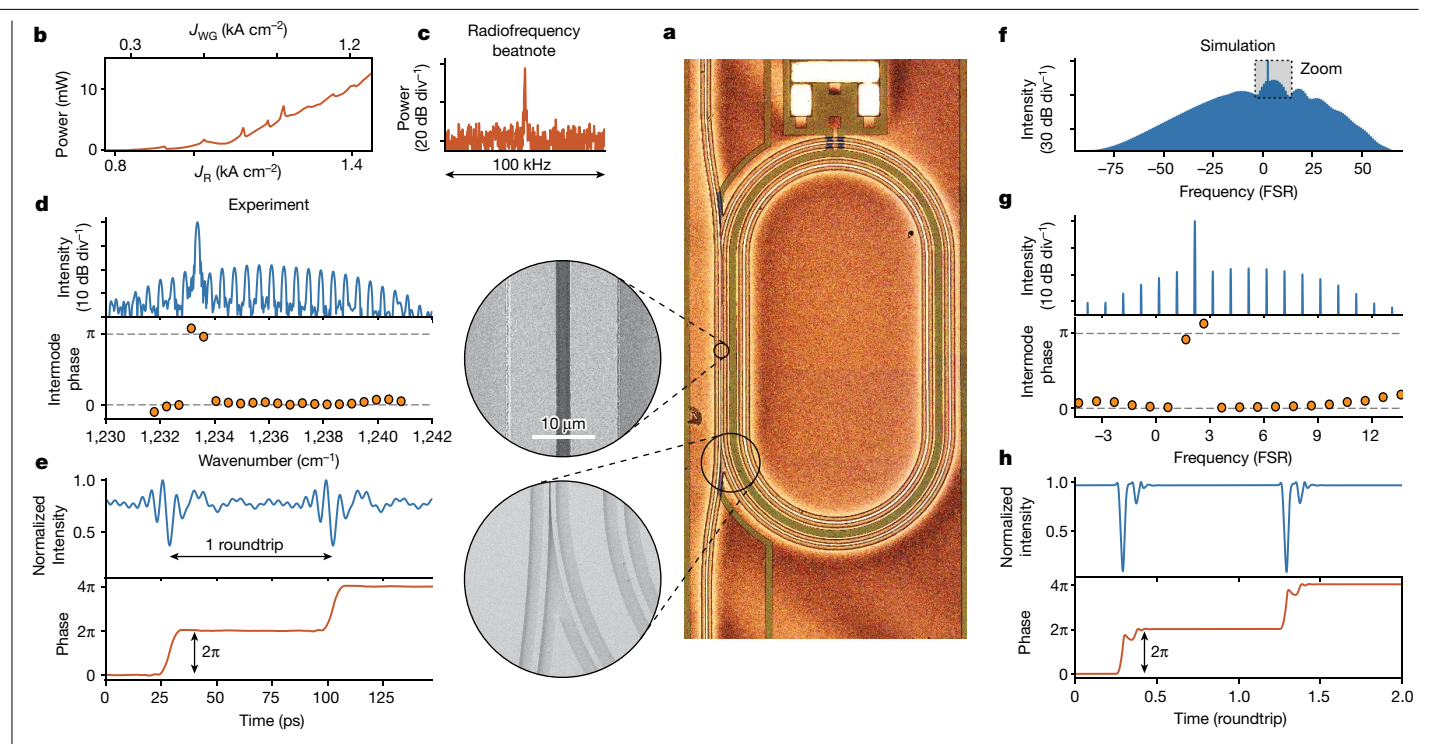


Fig. 2 | Experimental and theoretical characterization of fundamental NB solitons in a monolithic ring laser. a, Microscope image of the QCL ring and waveguide coupler, with separate electrical contacts. Scanning electron microscopy images depict the ring-waveguide coupling region. b, Output power of the device as a function of the ring and waveguide currents, J_R and J_{wg} , respectively. **c**, A narrow optical beatnote of the laser comb at a central frequency of 13.59 GHz, equal to the repetition frequency. d, Experimentally obtained intensity spectrum and the intermode phases of an NB soliton at bias currents of $J_R = 1.33 \text{ kA cm}^{-2}$ and $J_{WG} = 0.79 \text{ kA cm}^{-2}$. Intermode phases between weaker side modes are synchronized in-phase, while the phase of the primary $mode is \, \pi\text{-shifted.} \, Detailed \, SWIFTS \, measured \, data \, are \, presented \, in \, Supplementary \,$ Information. e, Temporal profiles of the intensity and phase of the emitted light. Within the width of the NB soliton, the phase changes its value by 2π and remains linear during the remainder of the roundtrip, confirming that the NB

soliton is surrounded by a single-frequency constant CW field. f,g, Intensity spectrum obtained from numerical simulations of the master equation (f) and zoomed-in top portion within the same range of 35 dB as the experimental spectrum in $\mathbf{d}(\mathbf{g})$. The π jumps around the primary mode—a salient characteristic of NB solitons—are visible in the intermode phases. h, The simulated temporal waveforms of the intensity and the phase over two roundtrips. A larger amplitude contrast compared with e is attributed to the limited dynamic range of detection in experiments, which results in a finite number of spectral modes used for the temporal waveform reconstruction. The simulated NB soliton is obtained for an LEF of 1.25, in agreement with typical values in QCLs³⁷. The cavity dispersion k'' was set to 800 fs² mm⁻¹, which together with the gain dispersion brings the total GVD value to about -700 fs² mm⁻¹ (see Supplementary Information for a discussion on different contributions to the effective GVD and nonlinearity in a laser).

is constant and contains a single optical frequency equal to that of the primary mode. Similar optical spectra have been observed in ref. 33 and discussed in relation to passive Kerr combs, however, leaving several open questions on the physical origin, in particular the missing connection to the required bistability, which in passive Kerr combs occurs due to the detuned injected single-mode pump. To corroborate our experimental findings in more detail, we employ numerical simulations of the master equation derived from the Maxwell-Bloch system (Supplementary equation (2))^{6,28} and introduce a paradigm for freerunning soliton formation, called NB solitons. The obtained comb spectrum, shown in Fig. 2f, has a smooth spectral envelope engulfing a strong primary mode and spanning more than 100 cavity modes. Numerical simulations are not constrained by a small dynamical range as in the experiment (around 35 dB in Fig. 2d). Hence, by concentrating on the top part of the simulated spectrum within the same range (Fig. 2g), we show a clear agreement with the experiment. The simulated intermode phases confirm the π shift between the primary mode and the side modes, indicating that this is a hallmark of NB solitons. The simulated temporal intensity in Fig. 2h matches the structures predicted by the CGLE theory in Fig. 1. In our numerical study, the NB solitons appear to be rather robust against small variations of the dispersive and nonlinear parameters. The soliton width, however, is strongly influenced by the gain bandwidth, which can be analytically shown via a rescaling law (Supplementary equation (13)). Higher-order dispersion due to the laser gainshape is the likely cause of the residual small ringing that trails the NB soliton, as is well known from microresonator solitons^{47,48}. The combined simulated and experimental temporal waveforms confirm that NB solitons are surrounded by a CW background-providing a compelling proof of their dissipative soliton nature.

Localization is another striking soliton feature, clearly noticed in multisoliton states-spontaneously ordered ensembles of several co-propagating solitons^{7,8}. Multisoliton states can be indubitably identified by their 'fingerprint' optical spectra, which have a modulated envelope due to the interference between individual solitons. Figure 3a depicts one such spectrum, consisting of smooth lobes with spectral holes in-between. The intermode phases indicate that, besides the usual π jumps around the primary mode, an additional π jump occurs at the position of the spectral hole, providing another telltale sign of a multisoliton state. The reconstructed intensity (Fig. 3b) shows two distinct dark pulses, during which the phase changes by 4π -twice as much as for a fundamental NB soliton. Master-equation simulations verify multisoliton states as well. The spectral behaviour, including the additional π intermode phase jump between the lobes, is seen in Fig. 3c. Other than enabling large amplitude contrast, the dynamic range of simulations allows to resolve the 4π change of the temporal phase in two steps, one for each soliton (Fig. 3e). Multistability is yet another crucial dissipative soliton trait predicted in Fig. 1. To emulate laser starting from spontaneous emission, weak noise from a random

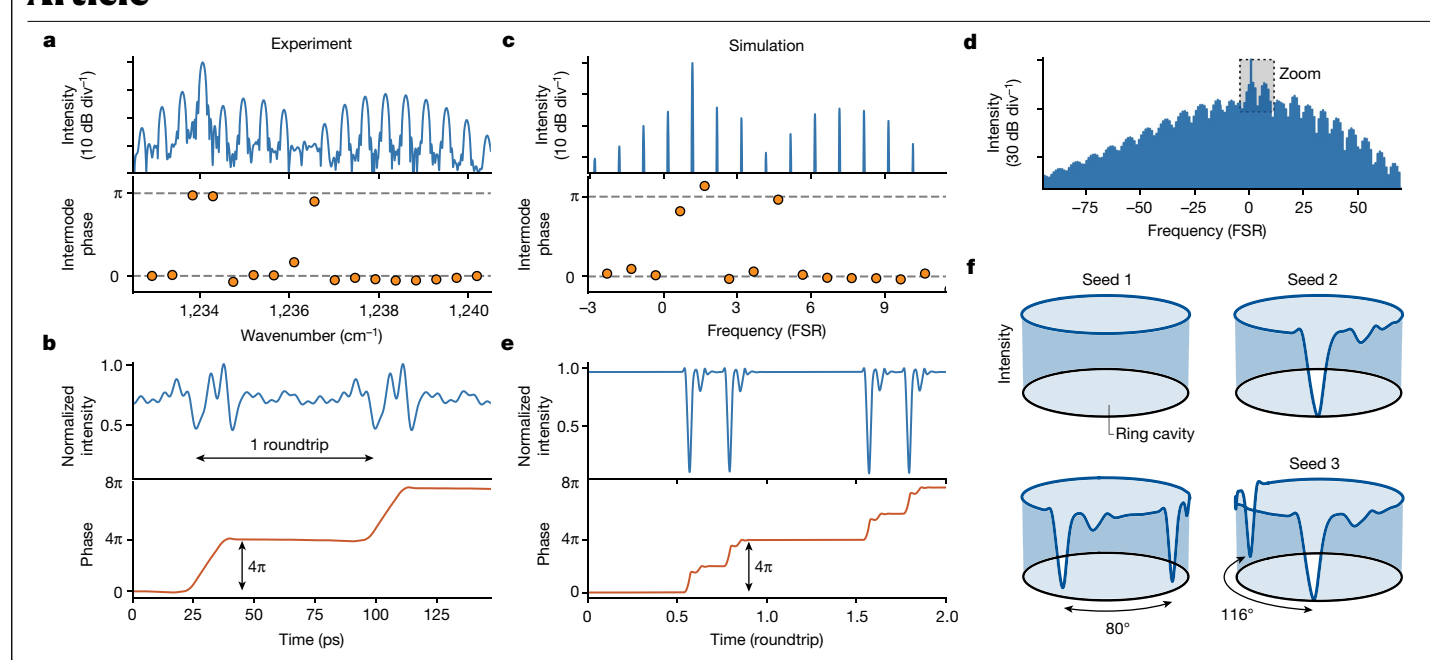


Fig. 3 | **Multisoliton states. a**, Spectral behaviour of an experimental multisoliton state, obtained for J_R = 1.28 kA cm⁻² and J_{WG} = 0.74 kA cm⁻². The interference between two NB solitons causes spectral modulation, resulting in smooth lobes separated by a spectral hole. The intermode phases indicate an additional π jump between the lobes. **b**, Two NB solitons appear in the intensity waveform, surrounded by a CW background. The temporal phase sweeps 4π within the two-soliton region. **c**, Zoomed-in top portion of the simulated spectrum and the intermode phases, in agreement with **a. d**, The intensity spectrum with the indicated zoomed-in section, shown in **c**. The spectral modulation, caused by the interference of the two solitons, cascades through the entire spectrum. **e**, Simulated temporal waveforms of the intensity and the phase. The larger dynamical range compared with the experiment allowed us

to distinguish two individual 2π ramps in the phase profile, one for each soliton. The LEF was set to 1.35 and k'' was set to 600 fs² mm⁻¹ (total GVD around -900 fs² mm⁻¹). **f**, Intracavity intensity profiles obtained for the same laser parameters when starting from different random noise conditions, labelled as seeds 1, 2 and 3. The coexistence of a CW single-mode field, a fundamental NB soliton and a multisoliton state verifies multistability and the fact that the laser operates in a linearly stable parameter region. The distance between the NB solitons in a multisoliton state is time invariant, but it changes for different laser parameters or starting conditions, as is seen from two states in the bottom row. The state in the bottom left is taken from **e**. Experimental evidence of a soliton crystal, which is a special case of multisoliton states where all of the solitons are equidistant¹⁵, is shown in Extended Data Fig. 1.

number generator with a defined seed is fed as a starting condition into the master equation (Methods). Changing the seed, while keeping other laser parameters fixed, led to three states with different number of solitons (Fig. 3f). The coexistence of solitons and a single-mode field proves that NB solitons are found in the CW linearly stable region of the parameter space, as predicted by the CGLE.

Separate electrical contacts of the waveguide and the ring provide two invaluable knobs for soliton control. Demonstrating this, we shift the soliton spectral lobe from the red side to the blue side of the primary mode purely by tuning the ring current in Fig. 4a. Besides changing the gain and the LEF^{10,28}, altering the bias strongly impacts the GVD, as confirmed by a coupled mode theory analysis of the ring-waveguide configuration (Fig. 4b,c). A small current-induced index mismatch between the ring and the waveguide induces large changes of the GVD, covering both normal and anomalous values. The key role of GVD is also obvious from numerical simulations in Fig. 4d, where we swept the cavity dispersion. Relative to the primary mode, the soliton is spectrally shifted similarly to Fig. 4a, and in agreement with recent observations in microresonators²¹. A more anomalous GVD sets the laser operating point in the linearly unstable parameter region in analogy to Fig. 1, where neither the single mode nor the NB soliton regime can exist. Instead, homoclons form via phase turbulence¹⁰, which we observe both in experiments and simulations (Supplementary Information).

Having the possibility to form bright pulses with high peak power would open many doors for NB solitons to be used in nonlinear processes, such as supercontinuum generation 45,49. One way of achieving this relies on modifying the phase of the primary mode to remove the destructive interference and induce an intense bright pulse. This could be realized by a second active ring resonator coupled with the

waveguide, acting as a notch filter⁵⁰. Another possibility in this direction is illustrated in Fig. 4e, where we show an NB soliton spectrum (in red), obtained at a larger bias compared with the soliton from Fig. 2 (replotted in blue). Astonishingly, the temporal intensity of the former reveals a low-contrast bright pulse. A comparison between the two soliton spectra reveals that the bright one has stronger side modes. To gain an intuitive understanding, Fig. 4f conceptually studies the dependence of the temporal intensity on the corresponding spectrum. while assuming the characteristic intermode phase distribution of NB solitons (see Supplementary Information for the full analysis). Whereas the primary mode is fixed, the soliton lobe is gradually increased, with the colour coding representing the two states from Fig. 4e. The initial increase of the soliton side modes enhances the amplitude contrast of a starting dark pulse, until an intensity equilibrium between the primary mode and the side modes is reached. At this point, destructive interference between the background and the soliton is complete and the dark pulse reaches zero at its minimum. Further enhancement of the side modes causes a decrease of the pulse amplitude contrast, eventually reaching a quasi-constant waveform despite a broad spectrum, as is also experimentally observed (Supplementary Information). Finally, additional side-mode amplification causes the pulse to 'flip over'-resulting in a bright coherent pulse. Both the CGLE and the master equation predict the emergence of NB solitons as dark pulses; however, neither of the two treatments takes into account the delayed carrier population response to amplitude modulations⁵¹. A better understanding of the link between the carrier dynamics and the parametric gain, which is necessary for multimode emission, could allow us to optimize active ring resonators for the emission of high-contrast bright pulses.

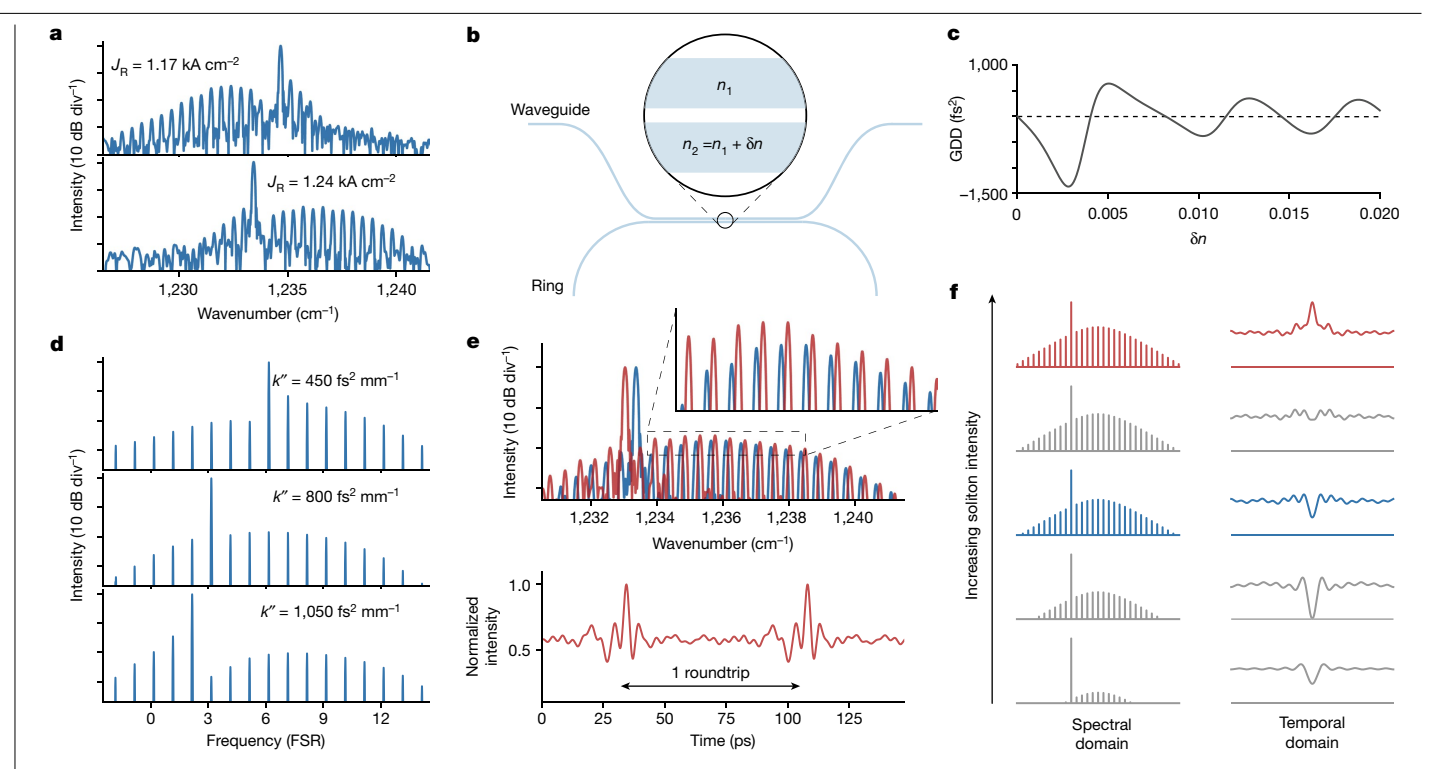


Fig. 4 | Coherent control of NB soliton regimes. a, Spectral shift of the soliton relative to the primary mode as the ring current is swept. Similar behaviour is exhibited if the waveguide current is tuned instead. A more detailed SWIFTS characterization is shown in Extended Data Fig. 2. b, Sketch of the coupled ringwaveguide system. The bias alters the optical indices of the ring (n_2) and the waveguide (n_1) through carrier- and thermal-induced changes, resulting in a mismatch $\delta n = n_2 - n_1$ (detailed analysis in Supplementary Information). c, Group delay dispersion (GDD), calculated with a coupled mode theory analysis, as a function of the index mismatch between the ring and the waveguide, which stems from different bias conditions (Supplementary Information). Compared

with a single ring cavity, our devices provide superior control of the dispersion. \mathbf{d} , Simulated soliton spectra as the cavity dispersion k'' is swept, demonstrating a spectral shift of the soliton similar to a. The gainshape contribution to the total GVD is around -1,500 fs² mm⁻¹. e, Experimentally obtained intensity spectrum of a NB soliton at bias currents of $J_R = 1.39 \text{ kA cm}^{-2} \text{ and } J_{WG} = 0.85 \text{ kA cm}^{-2} \text{ (red)},$ which corresponds to a bright pulse in the intensity waveform. The soliton side modes are stronger compared with the dark-pulse soliton from Fig. 2d $(replotted \, in \, blue). \, \textbf{\textit{f}}, Illustration \, of \, the \, theoretical \, dependence \, of \, the \, intensity$ waveform on the soliton spectrum. We assume ideal NB soliton intermode phase distribution with π jumps around the primary mode.

In this work, we have demonstrated a method of direct spontaneous soliton generation by utilizing an MIR semiconductor laser active material implemented in an on-chip integrated ring cavity with a coupler waveguide. The waveguide coupler has an independent bias, not only ensuring higher output powers but also providing a powerful knob to control the total dispersion of the system. Paired with the giant resonant Kerr nonlinearity of the active material, this solidifies the coupled waveguide-ring configuration as a fruitful playground for nonlinear phenomena—including the direct generation of electrically driven NB solitons. The soliton regime is demonstrated by combining both experimental and theoretical results. The number of solitons within one roundtrip varies stochastically with the initial conditions of the lasers. This is indicative of a multistability phenomenon, typical of dissipative solitons in extended systems, paving the way paving the way for independent addressing of individual solitons¹⁶.

The spontaneous formation of NB solitons with current tuning, without the need of an external optical pump, makes our QCL rings with coupled waveguides ideal candidates for monolithic soliton generators specifically targeting MIR applications. Even more striking, ring QCL NB soliton generators are by design intrinsically feedback insensitive and do not require optical isolators, which are very challenging to be realized on integrated platforms^{52,53}. This feature comes from the fact that wave propagation inside the ring resonator is unidirectional and the back-reflected light enters the cavity in the opposite direction. Light propagating in opposite direction is suppressed due to the stronger cross-saturation and only weakly couples to the soliton due to the lack of phase matching and reflection points in the cavity. This is in strong contrast to frequency-modulated combs from Fabry-Pérot lasers, where typically optical isolators are used to prevent the loss of coherence^{3,4,54}. An experimental comparison is shown in Extended Data Fig. 3 with a more detailed description provided in Methods.

Moreover, we predict that NB solitons are not platform dependent and anticipate their demonstration in other semiconductor laser types, such as the interband cascade or quantum-dot lasers. In any of these laser technologies, the gain material can also be used to realize integrated optical amplifiers and a second ring cavity could be used for spectral filtering of the primary mode. Hence, we propose a master-oscillator-power-amplifier configuration with an in-between spectral filter as an ideal configuration to boost the soliton power and significantly increase the usable comb bandwidth for applications.

Online content

Any methods, additional references, Nature Portfolio reporting summaries, source data, extended data, supplementary information, acknowledgements, peer review information; details of author contributions and competing interests; and statements of data and code availability are available at https://doi.org/10.1038/s41586-023-06915-7.

- Udem, T., Holzwarth, R. & Hänsch, T. W. Optical frequency metrology. Nature 416, 233
- Hugi, A., Villares, G., Blaser, S., Liu, H. C. & Faist, J. Mid-infrared frequency comb based on a quantum cascade laser. Nature 492, 229 (2012).
- Täschler, P. et al. Femtosecond pulses from a mid-infrared quantum cascade laser. Nat. Photon. 15, 919 (2021).

- Hillbrand, J., Andrews, A. M., Detz, H., Strasser, G. & Schwarz, B. Coherent injection locking of quantum cascade laser frequency combs. Nat. Photon. 13, 101 (2019).
- Villares, G. et al. On-chip dual-comb based on quantum cascade laser frequency combs. Appl. Phys. Lett. 107, 251104 (2015).
- Opačak, N. & Schwarz, B. Theory of frequency-modulated combs in lasers with spatial hole burning, dispersion, and Kerr nonlinearity. Phys. Rev. Lett. https://doi.org/10.1103/ physrevlett.123.243902 (2019)
- Herr, T. et al. Temporal solitons in optical microresonators, Nat. Photon. 8, 145 (2013).
- Guo, H. et al. Universal dynamics and deterministic switching of dissipative Kerr solitons 8. in optical microresonators. Nat. Phys. 13, 94 (2016).
- Xue, X. et al. Mode-locked dark pulse Kerr combs in normal-dispersion microresonators. Nat. Photon. 9, 594 (2015).
- 10. Piccardo, M. et al. Frequency combs induced by phase turbulence. Nature 582, 360 (2020).
- Meng, B. et al. Mid-infrared frequency comb from a ring quantum cascade laser. Optica 7. 11. 162 (2020).
- 12. Aranson, I. S. & Kramer, L. The world of the complex Ginzburg-Landau equation, Rev. Mod. Phys. 74, 99 (2002).
- 13. Bekki, N. & Nozaki, K. Formations of spatial patterns and holes in the generalized Ginzburg-Landau equation. Phys. Lett. A 110, 133 (1985).
- 14 Lega, J. Traveling hole solutions of the complex Ginzburg-Landau equation: a review. Physica D 152-153, 269 (2001).
- 15 Karpov, M. et al. Dynamics of soliton crystals in optical microresonators. Nat. Phys. 15, 1071 (2019).
- Akhmediev, N. & Ankiewicz, A. (eds) Dissipative Solitons: From Optics to Biology and 16. Medicine (Springer, 2008).
- 17 Grelu, P. & Akhmediev, N. Dissipative solitons for mode-locked lasers. Nat. Photon. 6, 84
- 18. Englebert, N., Arabí, C. M., Parra-Rivas, P., Gorza, S.-P. & Leo, F. Temporal solitons in a coherently driven active resonator. Nat. Photon. 15, 536 (2021).
- Leo, F. et al. Temporal cavity solitons in one-dimensional Kerr media as bits in an all-optical buffer. Nat. Photon. 4, 471 (2010).
- Rowley, M. et al. Self-emergence of robust solitons in a microcavity. Nature 608, 303 (2022).
- Zhang, S. et al. Dark-bright soliton bound states in a microresonator. Phys. Rev. Lett. https://doi.org/10.1103/physrevlett.128.033901 (2022).
- Marin-Palomo, P. et al. Microresonator-based solitons for massively parallel coherent optical communications. Nature 546, 274 (2017).
- 23. Riemensberger, J. et al. Massively parallel coherent laser ranging using a soliton microcomb. Nature 581, 164 (2020).
- Suh, M.-G., Yang, Q.-F., Yang, K. Y., Yi, X. & Vahala, K. J. Microresonator soliton dual-comb 24 spectroscopy, Science 354, 600 (2016).
- 25. Spencer, D. T. et al. An optical-frequency synthesizer using integrated photonics. Nature **557**, 81 (2018).
- Yao, Y., Hoffman, A. J. & Gmachl, C. F. Mid-infrared quantum cascade lasers, Nat. Photon. 26 6. 432 (2012).
- Williams, B. S. Terahertz quantum-cascade lasers, Nat. Photon, 1, 517 (2007).
- Opačak, N., Cin, S. D., Hillbrand, J. & Schwarz, B. Frequency comb generation by Bloch gain induced giant Kerr nonlinearity. Phys. Rev. Lett. https://doi.org/10.1103/ physrevlett.127.093902 (2021).
- 29. Friedli, P. et al. Four-wave mixing in a quantum cascade laser amplifier, Appl. Phys. Lett. 102, 222104 (2013).
- Gaeta, A. L., Lipson, M. & Kippenberg, T. J. Photonic-chip-based frequency combs. Nat. 30. Photon. 13, 158 (2019).
- Jaidl, M. et al. Comb operation in terahertz quantum cascade ring lasers. Optica 8, 780
- Paolo Micheletti et al. Terahertz optical solitons from dispersion-compensated antennacoupled planarized ring quantum cascade lasers. Sci. Adv. 9, eadf9426 (2023).
- Meng, B. et al. Dissipative Kerr solitons in semiconductor ring lasers. Nat. Photon. 16, 142

- Columbo, L. et al. Unifying frequency combs in active and passive cavities: temporal solitons in externally driven ring lasers. Phys. Rev. Lett. https://doi.org/10.1103/ physrevlett.126.173903 (2021).
- Prati, F. et al. Soliton dynamics of ring quantum cascade lasers with injected signal. Nanophotonics 10, 195 (2020).
- Henry, C. Theory of the linewidth of semiconductor lasers. IEEE J. Quantum Electron. 18, 259 (1982).
- Opačak, N. et al. Spectrally resolved linewidth enhancement factor of a semiconductor frequency comb. Optica 8, 1227 (2021).
- Efremidis, N., Hizanidis, K., Nistazakis, H. E., Frantzeskakis, D. J. & Malomed, B. A. Stabilization of dark solitons in the cubic Ginzburg-Landau equation. Phys. Rev. E 62, 7410 (2000)
- Perraud, J.-J. et al. One-dimensional "spirals": novel asynchronous chemical wave sources. Phys. Rev. Lett. 71, 1272 (1993).
- Burquete, J., Chaté, H., Daviaud, F. & Mukolobwiez, N. Bekki-Nozaki amplitude holes in 40. hydrothermal nonlinear waves, Phys. Rev. Lett. 82, 3252 (1999).
- 41. Slepneva, S. et al. Convective Nozaki-Bekki holes in a long cavity OCT laser. Opt. Express 27, 16395 (2019).
- Gowda, U. et al. Turbulent coherent structures in a long cavity semiconductor laser near the lasing threshold. Opt. Lett. 45, 4903 (2020).
- 43 Popp, S., Stiller, O., Aranson, I., Weber, A. & Kramer, L. Localized hole solutions and spatiotemporal chaos in the 1D complex Ginzburg-Landau equation. Phys. Rev. Lett. 70, 3880 (1993)
- Popp, S., Stiller, O., Aranson, I. & Kramer, L. Hole solutions in the 1D complex Ginzburg-Landau equation, Physica D 84, 398 (1995).
- Kazakov, D. et al. Active mid-infrared ring resonators. Nat. Commun. https://doi.org/ 10.1038/s41467-023-44628-7 (2024).
- Burghoff, D. et al. Evaluating the coherence and time-domain profile of quantum cascade laser frequency combs. Opt. Express 23, 1190 (2015).
- Jang, J. K., Erkintalo, M., Murdoch, S. G. & Coen, S. Observation of dispersive wave emission by temporal cavity solitons, Opt. Lett. 39, 5503 (2014).
- Anderson, M. H. et al. Zero dispersion Kerr solitons in optical microresonators. Nat. Commun. https://doi.org/10.1038/s41467-022-31916-x (2022).
- Obrzud, E., Lecomte, S. & Herr, T. Temporal solitons in microresonators driven by optical pulses. Nat. Photon. 11, 600 (2017).
- Liu, D., Zhang, L., Tan, Y. & Dai, D. High-order adiabatic elliptical-microring filter with an ultra-large free-spectral-range. J. Lightw. Technol. 39, 5910 (2021).
- Mansuripur, T. S. et al. Single-mode instability in standing-wave lasers: the quantum cascade laser as a self-pumped parametric oscillator. Phys. Rev. https://doi.org/10.1103/ physreva.94.063807 (2016).
- White, A. D. et al. Integrated passive nonlinear optical isolators. Nat. Photon. 17, 143-149 52. (2022).
- Xiang, C. et al. 3D integration enables ultralow-noise isolator-free lasers in silicon 53. photonics Nature 620, 78-85 (2023).
- Villares, G., Hugi, A., Blaser, S. & Faist, J. Dual-comb spectroscopy based on quantumcascade-laser frequency combs. Nat. Commun. https://doi.org/10.1038/ncomms6192 (2014)

Publisher's note Springer Nature remains neutral with regard to jurisdictional claims in published maps and institutional affiliations.

Springer Nature or its licensor (e.g. a society or other partner) holds exclusive rights to this article under a publishing agreement with the author(s) or other rightsholder(s); author self-archiving of the accepted manuscript version of this article is solely governed by the terms of such publishing agreement and applicable law.

© The Author(s), under exclusive licence to Springer Nature Limited 2024, corrected

Methods

Feedback-insensitive comb generation

Delayed optical feedback is a major issue in QCL frequency-comb applications. It destabilizes the laser output and impacts the nonlinear dynamics and coherence of the frequency-comb state⁴. Using optical isolators is one of the most common methods to prevent optical feedback. They must be employed in free-space tabletop systems, such as QCL-based dual-comb spectrometers and external pulse compressors^{3,54}. Downscaling these systems to integrated photonic chips requires alternative methods to mitigate the effects of back reflections from the downstream components^{52,53}. Here we show that ring QCL NB soliton generators are by design, intrinsically feedback insensitive. This feature comes from the fact that wave propagation inside the ring resonator occurs in only one direction, and the back-reflected light enters the cavity in the opposite direction. As the gain is strongly saturated by the unidirectional laser field, the back-reflected wave quickly dies out inside the resonator after entering it, having a minimal effect on the dynamics of the laser field. In a Fabry-Pérot laser, the field is bidirectional and will experience cross-gain saturation from the back-reflected radiation, destabilizing the laser state. It can be very clearly observed from the spectrogram of the intermode beatnote of such a Fabry-Pérot frequency comb subject to delayed optical feedback (Extended Data Fig. 3a). The beatnote loses coherence and experiences strong fluctuations for a wide range of feedback intensities. Ring QCLs generating unidirectional NB solitons are free of feedback-induced instabilities. The beatnote in the ring QCL remains coherent throughout the entire range of back-reflected intensities (Extended Data Fig. 3b). This fundamental feature makes ring QCLs potential rivals of Fabry-Pérot QCL combs in spectroscopy applications, especially for integrated solutions, such as on-chip dual-comb spectrometers⁵.

Device fabrication and operation

The used QCLs emit at around 8.2 μ m and consist of GalnAs/AllnAs layers on an InP substrate, with a band structure design based on a standard single-phonon continuum depopulation scheme. The waveguides and the narrow gap in the coupling region were etched using the standard fabrication recipe employing optical lithography. The waveguide width was 10 mm, the curved section of the racetrack was a semicircle with a radius of 500 μ m and the length of the straight section was 1.5 mm. The ring circumference defines the cavity repetition rate of around 13.6 GHz. The heat sink temperature was kept at 14 °C in all experiments.

Experimental set-up and characterization of the soliton states

The measurement of the spectral amplitudes and phases, which are used for the reconstruction of the temporal waveform, was done by utilizing the SWIFTS technique⁴⁶. An overview of the measurement procedure is provided in Supplementary Information. To record the laser output modulation at the repetition frequency, we employed a 50 GHz quantum-well infrared photodetector cooled to 77 K, originally purchased from Debut Optoelectronics together with a bias tee and a low-noise radiofrequency preamplifier. For beam collimation, we used a 8–12 µm anti-reflection-coated aspheric BD-2 lens with a focal length of 3 mm and a numerical aperture of 0.71 mounted on a high-precision 3-axis flexure stage from Thorlabs. The set-up used a custom-built high-resolution Fourier transform infrared spectrometer (about 500 MHz). A Zurich Instruments UHFLI lock-in amplifier was used for the acquisition of both the intensity and SWIFTS interferograms.

To stabilize the repetition frequency of the comb, we relied on electrical injection locking via a radiofrequency source. However, caution is required as using a too large injection power will perturb the soliton spectrum and its intermode phases, as can be seen in Supplementary Information. The light that is generated in and outcoupled from QCLs is transverse-magnetic polarized due to the selection rules of intersubband transitions within the conduction band.

Numerical simulations

Simulations of the CGLE were implemented using a pseudo-spectral algorithm coupled with an exponential time-differencing scheme. The master equation of a unidirectional field was discretized with a first-order forward finite-difference method. This method hugely benefits from parallel implementation on a graphics processing unit. cutting down the execution time by three orders of magnitude compared with a standard implementation on a central processing unit. As an example, we simulated tens of millions of time steps within minutes using an NVIDIA GeForce RTX 3070 graphics processing unit (tens of thousands of simulated cavity roundtrips are necessary to ensure that a steady state is obtained). To emulate a laser starting from spontaneous emission, the numerical simulations were run with random weak-intensity noise as a starting condition obtained from a random number generator with a defined seed value. Changing the seed results in a different randomly generated weak waveform, while preserving the mean intensity and variance. Weak noise is also added in the same way at every discretized cavity grid point after each time step.

Data availability

Source data are provided with this paper. Additional data that support the findings of this study are available from the corresponding authors upon reasonable request.

Code availability

Information on the code developed to simulate the QCL dynamics and its results are available from the corresponding authors upon reasonable request.

Acknowledgements This project has received funding from the European Research Council (ERC) under the European Union's Horizon 2020 Research and Innovation programme (grant agreement number 853014) and from the National Science Foundation under grant number ECCS-2221715. T.P.L. thanks the support of the Department of Defense (DoD) through the National Defense Science and Engineering Graduate (NDSEG) Fellowship Program.

Author contributions N.O., D.K., F. Pilat, T.P.L. and B.S. carried out the experiments and analysed the data. M.B. fabricated the device. N.O. performed the master-equation simulations. L.L.C., M.B. and F. Prati did the CGLE simulations and contributed to the analysis of the experimental results and their interpretation in the framework of the CGLE theory. N.O. prepared the paper with input from all co-authors. N.O., T.P.L., D.K. and F. Pilat wrote sections of the Supplementary Information. B.S., M.P. and F.C. supervised the project. All authors contributed to the discussion of the results.

Competing interests The authors declare no competing interests

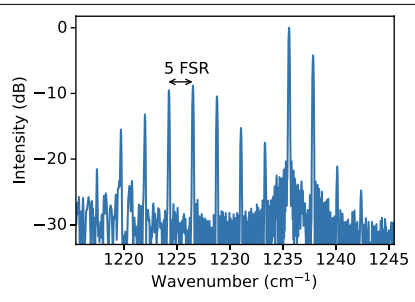
Additional information

Supplementary information The online version contains supplementary material available at https://doi.org/10.1038/s41586-023-06915-7.

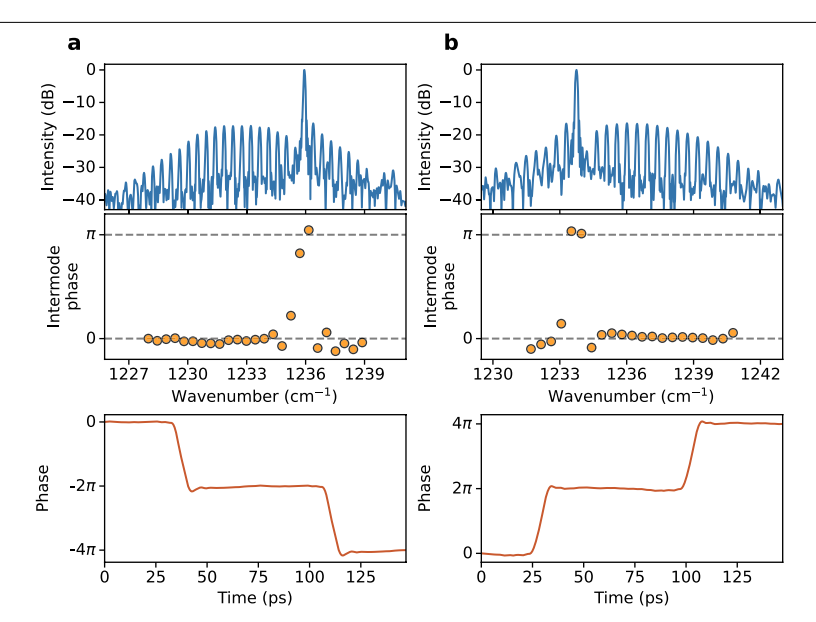
Correspondence and requests for materials should be addressed to Nikola Opačak or Benedikt Schwarz.

Peer review information Nature thanks Wenle Weng and the other, anonymous, reviewer(s) for their contribution to the peer review of this work. Peer reviewer reports are available.

Reprints and permissions information is available at http://www.nature.com/reprints.

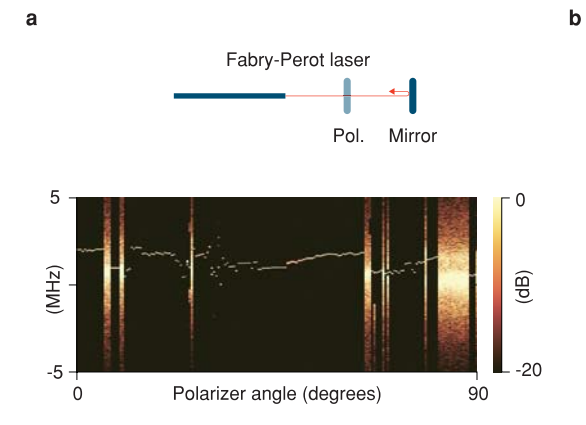


 $Extended\,Data\,Fig.\,1 |\, Experimental\,evidence\,suggesting\,an\,NB\,soliton$ crystal. Intensity spectrum of a probable fifth harmonic frequency comb, where the intermode spacing equals 5 FSRs. The soliton crystal regime is suggested by the smooth bell-shaped envelope of the spectrum. In the Fig. 3 of the main manuscript, we have shown an experimental and theoretical $characterization\,of\,a\,multisoliton\,state\,comprised\,of\,two\,co\text{-}propagating\,NB$ $solitons \, in \, a \, single \, round trip. \, A \, special \, case \, of \, multisolitonic \, states, \, where \,$ $all \, of the \, solitons \, within \, one \, roundtrip \, are \, equidistant, is \, called \, a \, soliton$ crystal¹⁵. In the frequency domain, these waveforms correspond to a harmonic frequency comb whose spacing between adjacent comb modes is equal to an integer multiple of the FSR: $N \times FSR$, where N is the number of solitons in the $soliton\,crystal.\,The\,coherence\,of\,the\,state\,is\,suggested\,by\,the\,high\,suppression$ ratio of the fundamental modes that fall beneath the noise floor, leaving only $the \, harmonic \, equidistant \, modes. \, Furthermore, the \, modes \, form \, a \, smooth$ bell-shaped spectral envelope that indicates the soliton nature of the state. The high frequency of the intermode beatnote (around 68 GHz) lies well $above \, the \, cutoff \, frequency \, of \, our \, optical \, detector, thus \, prohibiting \, SWIFTS$ characterization to truly assess the coherence of the state. This begs for the future use of another coherent technique to study soliton crystal dynamics in active ring resonators.

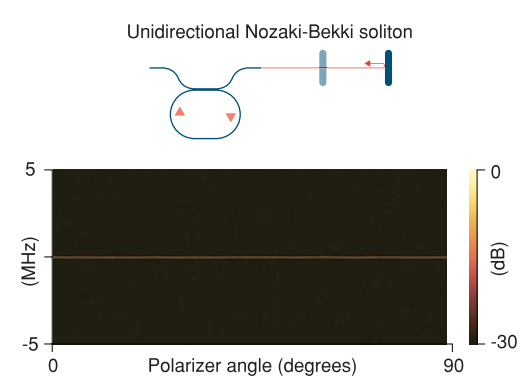


Extended Data Fig. 2 | **Shifting of the soliton spectral envelope relative to the primary mode.** Experimental characterization of two NB solitons where the tuning of the bias current results in a shift of the spectral soliton envelope from the red to the blue side of the primary mode (\mathbf{a} and \mathbf{b} respectively). The shift of the soliton spectral envelope happens as the currents of the ring and the waveguide are changed. The main reason for this likely lies in the large change of the total GVD, as discussed in the main manuscript, and recently observed experimentally in passive microresonators 21 . Although the soliton envelope may be positioned differently relative to the primary mode, the expected two π jumps of the intermode phases around the primary mode are

still present – indicating that this is indeed a salient feature of NB solitons. The temporal profile of the phase exhibits the familiar 2π ramp within the width of the soliton. We can observe that the direction of the ramp depends on whether the soliton spectral envelope is on the red or on the blue side relative to the primary mode. In a hypothetical state where the soliton envelope would be perfectly symmetric relative to the primary mode (if the soliton spectral center of mass coincides with the position of the primary mode), the 2π phase ramp would comprise two separate π ramps with an opposite direction. However, this state does not represent a stable fixed point, and is likely never to occur experimentally.



Extended Data Fig. 3 | Laser operation under delayed optical feedback. a, Fabry-Perot QCL spectrogram of the intermode beat note under delayed feedback induced by placing a mirror at the laser output. The feedback intensity is varied by rotating a polarizer placed between the laser facet and the mirror. The frequency axis of the spectrogram is centered at 5.833 GHz. **b**, Same



measurement as in $\bf a$, performed on a ring QCL generating a unidirectional Nozaki-Bekki soliton. The frequency axis of the spectrogram is centered at 18.623 GHz. In both measurements resolution bandwidth of the RF spectrum analyzer is $16\,\rm kHz$.